Magnetic loss versus temperature and role of doping in Mn-Zn ferrites

Journal of Magnetism and Magnetic Materials 603 (2024) 172228

Contents lists available at ScienceDirect

Journal of Magnetism and Magnetic Materials

journal homepage: www.elsevier.com/locate/jmmm

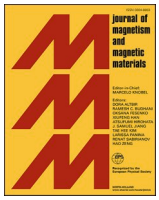

Research article

Magnetic loss versus temperature and role of doping in Mn-Zn ferrites

Vasiliki Tsakaloudi [a], Cinzia Beatrice [b,*], Fausto Fiorillo [b], Vassilios Zaspalis [a,c]

[a] Laboratory of Inorganic Materials, Centre for Research and Technology-Hellas CERTH, 57001 Thermi-Thessaloniki, Greece
[b] Advanced Materials Metrology and Life Science Division, Istituto Nazionale di Ricerca Metrologica, INRIM, 10135 Torino, Italy
[c] Laboratory of Materials Technology, Department of Chemical Engineering, Aristotle University of Thessaloniki, 54124 Thessaloniki, Greece

ARTICLE INFO

Keywords:
Mn-Zn ferrites
Magnetic losses
Magnetization process
High-frequency losses
Ferrite doping

ABSTRACT

We investigate the effect of different doping schemes on the broadband magnetic losses and their temperature dependence in Mn-Zn ferrites. CaO, Nb_2O_5, ZrO_2, and SiO_2 are added with increasing proportions to TiO_2-doped prefired powders and, after sintering at either 1275 °C or 1300 °C, the obtained ring samples are tested versus frequency f (DC-1 GHz) and peak polarization J_p (2 mT – 200 mT) up to $T = 160$ °C. Appropriately enhanced impurity contents are shown to induce further decrease of the energy loss in materials already prepared for best performance at high temperatures (140 – 160 °C). This behavior can be hardly ascribed to the impurity-related increase of the electrical resistivity brough about by extra-doping, being it rather connected to a corresponding monotonical decrease of the effective magnetic anisotropy $< K_{eff} >$ with T. The decreasing anisotropy makes the balance between the contributions of domain wall (dw) displacements and reversible rotations to the magnetization process evolving in favor of the latter. The energy loss correspondingly develops with frequency and peak polarization in a complex fashion, according to the specific dissipative mechanisms sustained by the spins precessing either inside the moving walls or in the bulk. A dividing line in the ($J_p - f$) plane is identified, which separates dominant dw- and rotation-generated losses. It moves downward (i.e. lower f) with increasing temperature, the higher T the lower the frequency at which the rotations, theoretically assessed via the Landau-Lifshitz equation, supersede the domain wall contribution. Once accomplished, however, the transition to rotations can lead, according to the theoretical model, to higher losses when moving to higher temperatures. Following the experimental trend of the complex resistivity versus frequency at different T values, the calculations and the experiments show that eddy currents start to contribute to the energy loss, in the 5 mm thick ring samples, around a few MHz, accounting for about 50 % of measured loss beyond some 50 MHz. The chief dissipative process at applicative frequencies and induction values is therefore identified with spin damping, to which the generalized loss decomposition method can be applied.

1. Introduction

The soft magnetic behavior of Mn-Zn ferrites can be modified and tailored to specific operating conditions of the cores by appropriate addition of extra-oxides to the host MnO-ZnO-Fe_2O_3 composition. Combined with flexibility in the preparation methods (from oxides mixing to sintering) and non-stoichiometry, the role of extra-cations can be fine-tuned and directed to the desired response of the material as a function of frequency and temperature. Soluble additives, like TiO_2 and CoO, enter the spinel matrix, modifying the intrinsic properties (e.g., the magnetocrystalline anisotropy), possibly interacting with little-soluble additives, like CaO, SiO_2, ZrO_2, and Nb_2O_5, to favor their segregation at the grain boundaries [1–4]. The role of the segregating cations is typically one of promoting vitrification and enhanced resistivity of the boundaries, thereby hampering the circulation of long-range eddy currents during the magnetization process [5–7]. Ti^{4+} and Co^{2+} cations tend to occupy the B-sites in the spinel structure, hindering electron hopping between Fe^{2+}-Fe^{3+}pairs and decreasing the intra-grain conductivity [1,8,9]. While Co^{2+} ions are effective in the process of anisotropy compensation and in the stabilization of the energy loss versus temperature [10,11], the dissolution of TiO_2 leads to Ti^{4+} and vacancy trail, favoring, in association with appropriate partial pressure of oxygen p_{O2} at the sintering stage, the diffusion of the dopant ions along the grain boundaries [1]. TiO_2 appears then to play a fundamental role in restraining the material conductivity, while being effective against magnetic aging, and its addition is welcome in Mn-Zn ferrite

* Corresponding author.
E-mail address: c.beatrice@inrim.it (C. Beatrice).

https://doi.org/10.1016/j.jmmm.2024.172228
Received 17 January 2024; Received in revised form 13 May 2024; Accepted 5 June 2024
Available online 6 June 2024

manufacturing [12,13]. However, the search for loss reduction by the mechanism of anisotropy compensation via the increase of the Fe^{2+}/Fe^{3+}cation ratio, as obtained by regulating p_{O2}, can lead, in the absence of Co^{2+}, to minimum value of the energy loss W at relatively low temperatures, below $T = 100$ °C, followed by a rapid increase versus T [12]. The problem is therefore posed about the possibility to achieve minimum and low loss figure at higher temperatures (say around 150 °C) by acting both on the sintering parameters and the doping scheme, with the objective of moving the compensation point upward, while contrasting the drop of the material resistivity with T. This can be rationally attempted in the framework of comprehensive magnetic and electric characterization of the material, possibly sustained by physical modeling.

In this work we investigate the electric and magnetic properties of power Mn-Zn sintered ferrites, enriched by addition of 2000 ppm TiO_2 and of CaO, SiO_2, ZrO_2, and Nb_2O_5 in increasing proportions. A wide-band magnetic characterization (DC – 1 GHz) across the polarization range 2 mT $\leq J_p \leq$ 200 mT is made, in association with resistivity measurements, from room temperature up to $T = 160$ °C. Ring samples of average diameter 12 mm and thickness ~ 5 mm are tested versus frequency by combination of fluxmetric and transmission line methods. The results are analyzed first by identifying and calculating the eddy current loss, making use of the resistivity behavior measured versus frequency and temperature and with the help of the magnetic characterization of thinned samples. The singled-out loss contribution is shown to take hold only beyond a few MHz in the 5 mm thick samples. It amounts to about 50 % of the measured loss beyond $f \sim 50$ MHz and it is concluded that it can be appreciated below 1 MHz only in quite large samples [14]. The present investigation, stretching from quasi-static excitation to frequencies so high as to achieve full permeability relaxation, can actually provide an exhaustive experimental landscape, against which a comprehensive physical approach can be validated. This contrasts with the somewhat restricted span of frequencies of power applications and the related experiments [15]. Physical modeling, emerging from the analysis of the magnetization process and lumped in a generalized formulation of the Statistical Theory of Losses (STL) [16,17], can provide a general interpretative framework, going beyond phenomenologically oriented loss formulations (e.g., the Steinmetz's model and its many variants [18,19]). We therefore focus on the properties of the magnetization process and the way the motion of the domain walls (dws) and the rotation of the spins in the bulk evolve and combine as a function of frequency and temperature. Following the STL guided approach discussed in previous studies [17,20], we can discriminate between these two magnetization processes, which are shown to correlate with the excess $W_{exc}(f)$ and classical $W_{class}(f)$ dynamic loss components, respectively, the hysteresis (quasi-static) component W_{hyst} being exclusively associated with the motion of the dws. Once the eddy current losses are singled out, we are left with spin damping as the dissipating mechanism and we write the related magnetic energy loss decomposition as

$$W_{sd}(f) = W_{dw}(f) + W_{rot,sd}(f) = W_{hyst}(f) + W_{exc,sd}(f) + W_{rot,sd}(f), \quad (1)$$

where, making abstraction of eddy currents, $W_{rot,sd}(f)$ plays the role usually assigned to $W_{class}(f)$, given the quasi-homogeneous character of the rotations in the bulk. It is the evolving balance between dw displacements and rotations with frequency the key to the overall broadband loss response of Mn-Zn ferrites. These processes ultimately depend on the effective anisotropy constant K_{eff} and its distribution across the multitude of grains, so that any treatment leading to a change of this quantity will engender a change of their relative proportions. Quite generally, we can refer to a $K_{eff}^{1/2}$ and a K_{eff} dependence for the dw and rotational (anisotropic) energies, respectively. Any increase of temperature, at least up to the compensation point, will therefore favor the rotations versus the dw displacements. Moving towards higher compensation temperatures implies maximum rotational contribution at such temperatures. This does not imply that $W_{rot,sd}(f)$ is a decreasing function of T. In fact, it is not, given its resonant origin. Only at sufficiently high J_p values (typically $J_p > 50 – 100$ mT) and prevalent dw contribution to the magnetization reversal, one can observe loss decrease with increasing T. It is eventually found that, by a 20 % increase of the base content of CaO, ZrO_2, and Nb_2O_5 and the additional introduction of 50 ppm SiO_2, the energy loss at such J_p values suffers a 20 % – 30 % decrease at temperatures above 100 °C

Table 1
Dopant contents and sintering temperature T_s of the investigated Mn-Zn ring samples. The standard concentrations of CaO, Nb_2O_5, and ZrO_2 are in the proportion 3:1:1.

Dopants	Sample D1	Sample D4	Sample D4S1	Sample D4S1n	Sample D4S2
	T_s = 1300 °C	T_s = 1300 °C	T_s = 1275 °C	T_s = 1300 °C	T_s = 1275 °C
TiO_2 (ppm)	2000	2000	2000	2000	2000
CaO (ppm)	standard	+ 20 %	+ 20 %	+ 20 %	+ 20 %
Nb_2O_5 (ppm)	standard	+ 20 %	+ 20 %	+ 20 %	+ 20 %
ZrO_2 (ppm)	standard	+ 20 %	+ 20 %	+ 20 %	+ 20 %
SiO_2 (ppm)	–-	–-	50	50	100

2. Preparation and characterization of the Mn-Zn samples

Four batches of Mn-Zn ferrites consisting of 71 wt% Fe_2O_3, 23 wt% MnO and 6 wt% ZnO were synthesized following the conventional solid-state processing. High-purity raw material oxides (Fe_2O_3 provided by the industrial supplier Thyssen-Krupp. Analytical Grade, ZnO and MnO, provided by Merck, were weighed into the appropriate amounts at 850 °C for 4 h. Dopants were added prior to 9-hour milling by steel balls in steel vessels, with water as the suspension medium. Table 1 provides the doping scheme of the investigated samples, where, besides a constant TiO_2 = 2000 ppm content, the base CaO, ZrO_2, and Nb_2O_5 concentration in sample D1 is increased by 20 % in D4 and further enriched by 50 ppm SiO_2 in D4S1 and D4S1n. 100 ppm SiO_2 are finally added to D4S2. After drying at 90 °C for 24 h and sieving of the milled powder (average particle size 0.56 ± 0.05 μm), roll granulation was performed using 0.2 wt% polyvinyl alcohol as a binder. Compaction of toroidal samples to the average density of 2.90 ± 0.02 g/cm^3 was performed by uniaxial pressing. Sintering of the compacted specimens, leading to complete ferrite formation, was performed at either 1300 °C or 1275 °C for 3 h in specially constructed kilns, where the partial pressure of oxygen is controlled according to the Morineau and Paulus equation. The preparation process is sketched in the flowchart shown in Fig. 1. The final ring samples are about 5 mm high, with 15 mm outer diameter and 9 mm inner diameter. X-Ray Diffraction of the prefired powders revealed that primary nuclei of spinel structure have been formed during the prefiring step, while the examination of the crystal structure of the sintered specimens confirmed that all samples are pure spinel phases. The SEM analysis showed that the average grain size slightly increased from D1 to D4 (Table 2), with relatively narrow distribution in both cases. The introduction of SiO_2 into the D4 version (samples D4S1, D4S1n and D4S2) leads to significantly wider grain size distribution around a smaller mean grain size. The SiO_2-doped samples carry the microstructural characteristics that act as precursors of secondary recrystallization when higher sintering temperatures are applied. They exhibit remarkably higher DC resistivity with respect to samples D1 and D4 (Table 2), pointing to an effective role of Si^{4+} segregation at the grain boundaries.

After 2-hour stabilization annealing at 185 °C, the sintered ring samples, whose actual thickness ranged between 5.02 mm and 4.40 mm,

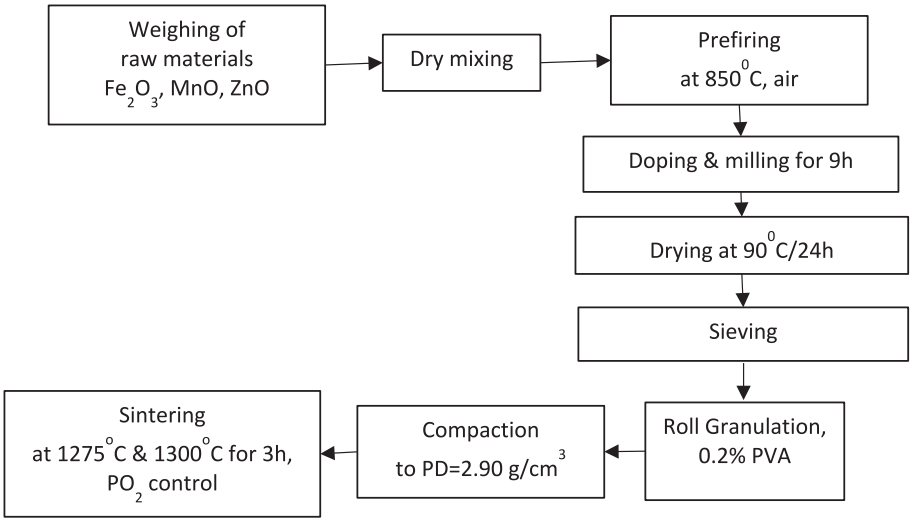

Fig. 1. Processing scheme of the Mn-Zn ferrites.

Table 2
Structural, electric, and magnetic parameters of the investigated Mn-Zn ring samples. δ ≡ mass density; <*s*> ≡ average grain size; $\rho_{DC,23}$, $\rho_{DC,160}$ ≡ DC resistivity at 23 °C and 160 °C; $\sigma'_{10M,23}$, $\sigma'_{10M,160}$ ≡ real conductivity at 10 MHz and at 23 °C and 160 °C. $J_{s,23}$, $J_{s,160}$ ≡ saturation magnetization at 23 °C and 160 °C.

Sample	δ (kg/m³)	<*s*> (μm)	$\rho_{DC,23}$ (Ωm)	$\rho_{DC,160}$ (Ωm)	$\sigma'_{10M,23}$ ($\Omega^{-1}m^{-1}$)	$\sigma'_{10M,160}$ ($\Omega^{-1}m^{-1}$)	$J_{s,23}$ (T)	$J_{s,160}$ (T)
D1	4733	8.6	6.31	0.447	48.4	42.5	0.529	0.300
D4	4767	9.5	5.14	0.525	44	40.8	0.532	0.308
D4S1	4807	7.5	8.24	0.516	49.6	36.9	0.536	0.302
D4S1n	4837	8.7	7.89	0.644	50	43.1	0.539	0.305
D4S2	4810	7.8	10.3	0.80	46.1	38	––	––

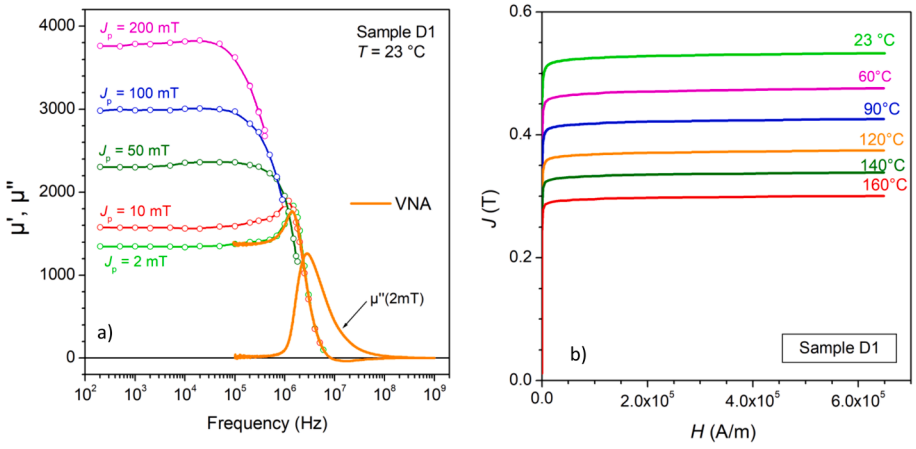

Fig. 2. A) example of measured broadband permeability behaviour at room temperature. the symbols show the results of fluxmetric measurements. the solid lines (μ' and μ'') are obtained by the transmission line method (VNA). b) Normal magnetization curves measured up to saturation between 23 °C and 160 °C with the Vibrating Sample Magnetometer method.

were subjected to electric characterization up to 15 MHz by four-wire impedance measurements. Voltmetric and amperometric electrical contacts were made on a cut ring sample (~5 mm gap) by sandwiching, close to the gap, indium strips between the polished sample surface and the four copper leads and applying uniform pressure. The measurements were made using an Agilent 33220A function generator and a 350 MHz, 2.5 GS/s TDS5034 oscilloscope, and the results were checked by means of an impedance analyzer Agilent 4294A. The saturation polarization was measured up to $T = 160$ °C by testing 3 mm diameter spherical samples with a Vibrating Sample Magnetometer and maximum effective field of 700 kA/m (Fig. 2b). The spherical samples were ground from the same batch of sintered rings used for the fluxmetric measurements. A calibrated digital wattmeter-hysteresis graph with NF HSA 4101 high-speed power amplifier was employed for the fluxmetric characterization, carried out from DC (normal magnetization curve) up to the maximum frequency of 10 MHz. The number of primary and secondary windings (0.25 mm wire diameter) and their arrangement evolved with frequency, with suitable overlapping intervals, to minimize the effect of the stray parameters. Starting from a few hundred kHz, the fluxmetric characterization partially overlapped with the transmission line measurement of the complex permeability via the determination of the scattering parameters in reflection and sweep mode by means of a VNA

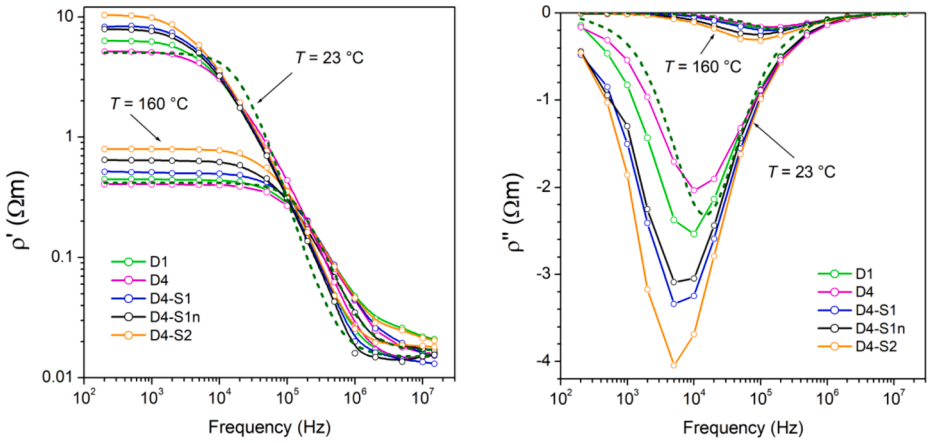

Fig. 3. Real ρ'and imaginary ρ''resistivity components versus frequency at 23 °C and 160 °C. They are obtained by four-wire impedance measurements, performed up to 15 MHz. Their behavior can be simulated by adopting the usual equivalent RC circuit, with the grain resistance R_g in series with the parallel of grain-boundary resistance R_b and capacitance C_b, according to Eq. (2) (see Fig. 4a). The accuracy of the fitting by Eq. (2) (dashed lines, applied to sample D4) can be improved by assuming a distribution of the involved time constant.

analyzer (Rhode & Schwarz mod. ZNB8) up to 1 GHz. The ferrite ring sample is placed at the bottom of a shorted coaxial line, under constant incident power $P = 10$ mW. A discussion on the fluxmetric and VNA methods and their combination in the characterization of soft ferrites is given in [21]. It is remarkably found that the fluxmetrically and VNA measured magnetic quantities eventually merge, the higher the J_p value the higher the frequency at which merging occurs. At such frequencies, the dw contribution to the magnetic losses is dwarfed by the rotations. An example of broadband permeability behavior, measured across a range of J_p values, is shown in Fig. 2a. To note the overlap of the VNA and fluxmetrically obtained real permeability μ'(f) curves across the common high-frequency range.

3. Experimental and discussion

In this Section we highlight the main results concerning the evolution of the electrical and magnetic properties of the TiO_2- enriched Mn-Zn ferrites under increased doping by Ca, Nb, Zr, and Si oxides. We shall clarify the role of eddy currents on the high-frequency loss response of the material, eventually tracing the overall behavior of the material versus frequency and temperature to the evolution of the effective anisotropy. Its fundamental role in balancing, via the spin damping mechanism, the competing contributions of rotations and dw displacements to the magnetization reversal, with prominent effects on the energy losses, is emphasized.

3.1. Electrical properties versus frequency and temperature. Eddy current losses

The dependence of the real ρ'(f) and imaginary resistivities ρ''(f), as derived from the electrical impedance measured at 23 °C and 160 °C, is summarized in Fig. 3. The represented quantities pertain to the electrically equivalent homogeneous material of impedance $Z = R_s - jX_s$ and, for a measurement made on a sample of length l_m and cross-sectional area S, we get

$$\rho' = R_s S/l_m \qquad \rho'' = X_s S/l_m \tag{2}$$

We lump in Eq. (2) the actual heterogeneous response of the grain boundaries and the grains (having resistivity of the order of 10^5 Ωm and 10^{-2} Ωm, respectively), which form a complex network of resistors (the

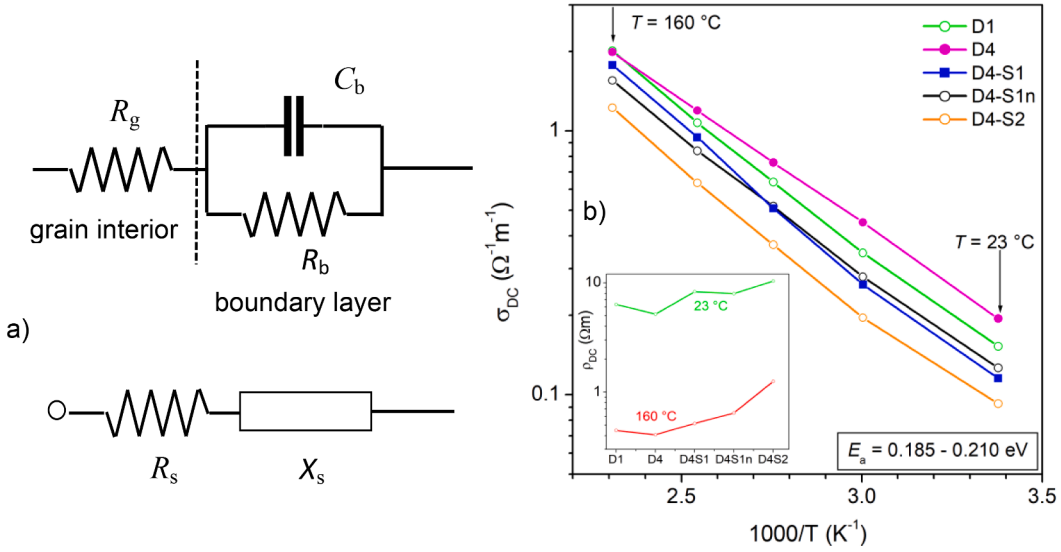

Fig. 4. a) Simplified electrical model of the Mn-Zn sintered ferrite, lumping the network of grains and grain boundaries in the series-connection of resistance R_s and reactance X_s of the equivalent homogeneous material. b) The DC conductivity of the ferrites σ_{DC} increases with temperature according to an activation law, with the activation energy E_a ranging between 0.185 eV and 0.213 eV. The inset shows the evolution of the DC resistivity ρ_{DC} with doping at 23 °C and 160 °C.

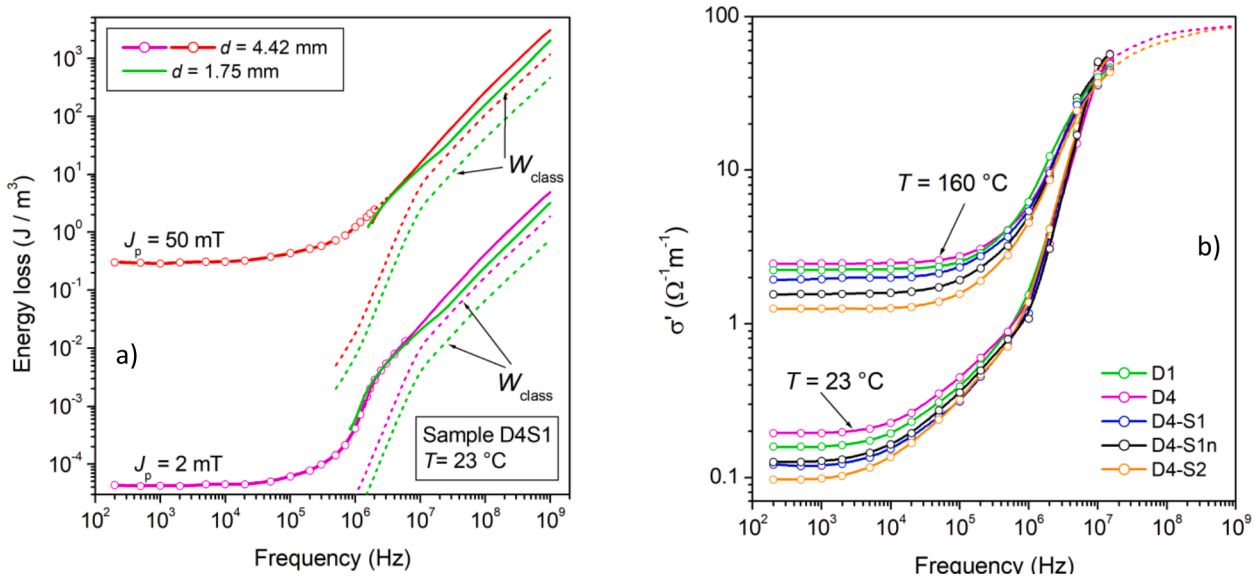

Fig. 5. a) The energy loss is not affected by eddy currents below about 5 MHz in the present samples, as shown by the coalescence of the $W(f)$ curves measured before and after sample thinning (from $d = 4.42$ mm to $d = 1.7$ mm). At such high frequencies, the observed decrease of $W(f)$ upon thinning corresponds with good approximation with the decrease of $W_{class}(f)$, as calculated for the two d values with Eq. (4) (dashed lines). The curves with open symbols and the continuous lines, overlapping at intermediate frequencies, are obtained by fluxmetric and VNA measurements, respectively b) Real conductivity $\sigma'(f)$ at 23 °C and 160 °C. This quantity tends to a temperature and sample independent value at the highest frequencies.

grains) and capacitors (the boundaries) with a very large resistance in parallel [22]. A drastic simplification consists in reducing this array to a simple RC circuit,

$$R_s = R_g + R_b/(1+\omega^2 R_b^2 C_b^2) \qquad X_s = \omega R_b^2 C_b/(1+\omega^2 R_b^2 C_b^2) \tag{3}$$

where R_g and R_b represent the grain and grain boundary contributions to the sample resistance, respectively, and the capacity C_b belongs to the grain boundaries (Fig. 4a). Eq. (3) fits the gross features of the dependence of $\rho'(f)$ and $\rho''(f)$ on frequency (dashed lines in Fig. 3). The order of magnitude decrease of the DC resistivity ρ_{DC} observed on passing from room temperature to $T = 160$ °C reveals the semiconducting properties of the grain boundary layer. It is associated, according to Eq. (3), with a shift of the maximum value of $\rho''(f)$ towards high frequencies. By plotting the conductivity $\sigma_{DC} = 1/\rho_{DC}$ versus $1/T$, we find (Fig. 4b) the law $\sigma_{DC} = \sigma_0 \exp(-E_a/k_B T)$, with the activation energy E_a falling in the range 0.185 eV − 0.210 eV, in agreement with previous literature [23]. The effect of increased doping on ρ_{DC} at 23 °C and 160 °C is shown in the inset of Fig. 4.

We wish to know how the knowledge of the electrical response of Mn-Zn ferrites can be exploited in calculating the eddy current losses and their dependence on frequency. It is widely assumed that the increase of the resistivity engendered by the segregation of dopants at the grain boundaries brings about a major advantage in terms of losses. However, the phenomenology of $\rho'(f)$ and $\rho''(f)$ shown in Fig. 3 and the actual evolution of the eddy current patterns from the grain interior to the whole sample cross-section under increasing frequency complicate the calculation of the eddy current losses. Such calculation basically regards the classical loss $W_{class}(f)$, the quantity one would obtain assuming identical local and macroscopic induction derivative (absence of dws). We find here that the motion of the dws is basically constrained by the grain boundaries, imposing a limitation on the related eddy-current damping coefficient β_{ec}, which is dwarfed by the spin-damping coefficient β_{sd}. We obtain, in fact, that, for a single dw moving inside a grain of size $< s >$, $\beta_{ec} = 4\sigma_g G J_s^2 \langle s \rangle$ [24] and $\beta_{sd} = 2J_s\alpha/\mu_0\gamma\delta$ [25], where σ_g is the conductivity of the grain, $G = 0.1356$, J_s is the saturation polarization, α is the Landau-Lifshitz damping constant, γ is the electron gyromagnetic ratio, and δ is the dw thickness. It is obtained that, with the parameters pertaining to the investigated ferrites, β_{sd} is two- three orders of magnitude higher than β_{ec}. We can therefore limit our analysis of the eddy current losses to $W_{class}(f)$, which we can do both by calculation and experiment. The calculation is made complex by the heterogeneous structure of the ferrites, where the eddy current patterns progressively evolve with frequency from the grain interior to the whole sample cross-section. Based on a specific multiscale model, a closed formulation for $W_{class}(f)$ covering this scenario was proposed [14], but the problem is conveniently simplified by measuring the broadband losses on samples of different thickness, where the sole dependence on the sample cross-sectional area and aspect ratio are involved. Fig. 5 illustrates how $W(f)$ is affected by thinning (from $d = 4.42$ mm to $d =$ to 1.75 mm) in the D4S1 sample at room temperature. The decrease of $W(f)$ upon thinning starts once the frequency is increased beyond about $f = 5$ MHz. It appears that the role of eddy currents can be appreciated below the MHz range only in much larger samples, as discussed in [14], where it is shown that one can calculate an upper limit $W_{class}(f)$ using the standard formulation for a homogeneous material. This is given, for a sample having rectangular cross-section of area S and aspect ratio R, by the equation

$$W_{class}(f) = \frac{\pi^2}{6} \bullet (12k(R)S) \bullet \sigma'(f) J_p^2 f \ [\mathrm{J/m^3}] \tag{4}$$

where $k(R) = 0.036 \cdot (1\text{-}\exp(R/0.32))$ [26], and

$$\sigma'(f) = \rho'(f)/(\rho'(f)^2 + \rho''(f)^2) \tag{5}$$

To note that the standard formulation, where $W_{class}(f)$ in ferrites is taken proportional to the square of the sample thickness [2,3], is quite at odds with the geometry of the conventional ring samples, whose aspect ratio is generally not far from 1. The experimental frequency dependence of $\sigma'(f)$ in the investigated samples, shown in Fig. 5b for $T = 23$ °C and 160 °C, puts in evidence the trend towards coalescence of all the $\sigma'(f)$ curves beyond about 5–10 MHz, independent of sample type and temperature. Such a trend, descends from concomitant vanishing of $\rho''(f)$, as observed in Fig. 3b, implying $\sigma'(f) \sim 1/\rho'(f)$, and the apparent minor role of doping on the high-frequency resistivity of the semiconducting grains. Coalescing electrical impedance values at high frequencies, independent of doping and temperature, are typically observed in Mn-Zn sintered ferrites [27,28]. The dashed lines in Fig. 3a,

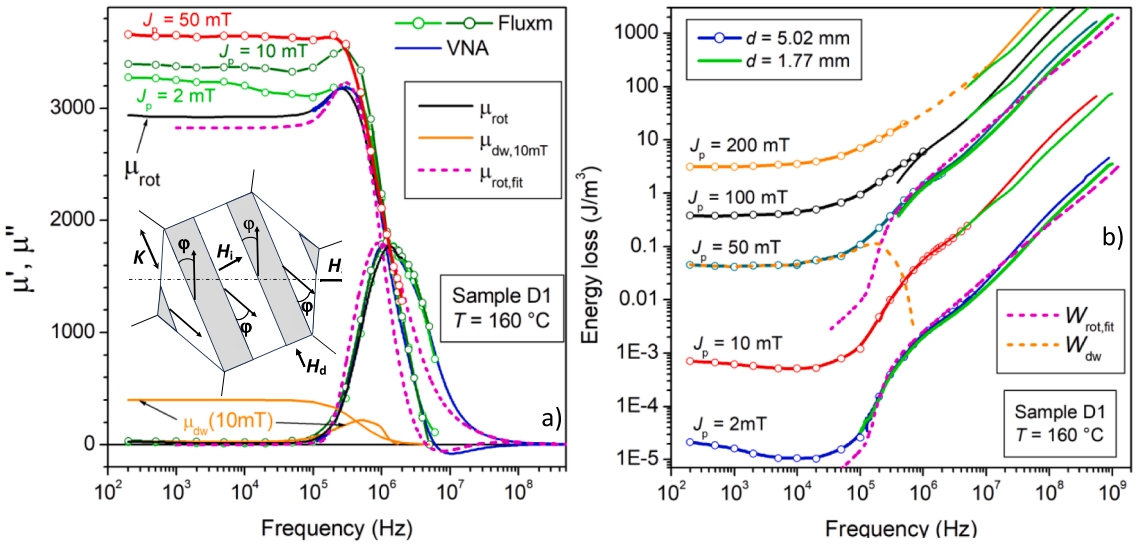

Fig. 6. a) An example of experimental complex permeability measured at three different J_p levels in the sample D1 at 160 °C. Its analysis permits one to discriminate between the rotational and dw components. The latter (μ'_{dw} and μ''_{dw}) are shown here for $J_p = 10$ mT, in association with the rotational contribution (μ'_{rot} and μ''_{rot}). A contribution to μ'_{dw} by the after-effect is apparent for $J_p = 2$ mT at the lowest frequencies. The increase of the permeability with J_p, all due to the dw processes, tends to disappear at high frequencies, consistent with the merging of the experimental curves. The dashed lines are the predicted behaviors of μ'_{rot} and μ''_{rot}. The inset provides a model for the magnetization process inside a grain having easy axis generically misoriented with respect to the applied field. b) Corresponding loss behavior in the J_p range 2 mT – 200 mT. The continuous lines, obtained by the VNA method, overlap with the fluxmetric curves in a large frequency interval at low J_p. The green lines are obtained on the thinned rings. The dashed lines represent the theoretically calculated rotational loss by spin damping $W_{rot,sd}(f)$ and the loss contribution by the moving dws $W_{dw}(f)$ for $J_p = 50$ mT. To note the loss contribution by the diffusion aftereffect for $J_p = 2$ mT and $f < 10$ kHz. (For interpretation of the references to colour in this figure legend, the reader is referred to the web version of this article.)

calculated by Eq. (4), quantitatively justify the decrease of $W(f)$ with decreased thickness and the bifurcation of the $d = 4.42$ mm and $d = 1.75$ mm curves at high frequencies. The problem becomes then one of assessing the loss generated by the mechanism of spin damping.

3.2. Domain wall motion versus spin rotations

The magnetization process in low- and vanishing-anisotropy soft magnetic materials (e.g. soft ferrites, amorphous and nanocrystalline ribbons, etc.) is usually shared by the rotation of the spins inside the domains and the motion of the dws. Since the rotations can only occur reversibly in these materials, one can conclude, in general, that the losses are always reduced, for a same J_p value, by an increased proportion of rotations with respect to the dw displacements. This statement is easily justified when one looks at the largely different degree of localization in space and time of the magnetization reversal if either the dws or the bulk of the domains are involved. With the former we have $\Delta J \sim 2J_s$ occurring at the wall coordinate and much larger dJ/dt with respect to the latter, which compounds with the squared dependence of the energy loss on the eddy current density [16]. While this is certainly true when the eddy current losses are involved, it may occur up to a certain extent only if, like in the Mn-Zn ferrites, spin damping becomes the prevalent dissipation channel. The balance between these two competing processes evolves in sintered ferrites with J_p and the frequency, with the rotations, favored by increasing f, providing their maximum contribution to the reversal around the demagnetized state. It is expected, in particular, that the dw permeability $\mu_{dw}(f)$ will suffer earlier relaxation with respect to $\mu_{rot}(f)$, because of the quite larger frictional torque sustained by the spins precessing inside the walls, compared to those precessing inside the domains. Such a torque can be expressed, according to the Gilbert equation, as

$$|\Gamma| = \left(\frac{\alpha}{\gamma M_s}\right)\left|\boldsymbol{M} \times \frac{d\boldsymbol{M}}{dt}\right| = \left(\frac{\alpha}{\gamma\mu_0}\right)J_s\frac{d\theta}{dt} \quad (6)$$

where $\boldsymbol{M}$ is the magnetization vector and $d\theta/dt$ is the angular velocity of the precessing spins. There is an obvious large difference between $d\theta/dt$ inside the wall and inside the domains and it is clear that the much faster rotations in the walls engender much larger frictional torque Γ on the moving dws, making the rotations in the bulk increasingly favored under increasing frequencies. This additionally implies that the dw resonance, if any, can only play a negligible role, both because of the rapidly declining role with frequency of the dw displacements with respect to the rotations (for any given J_p value) and because the dw relaxation frequency is expectedly lower than the dw resonance frequency [29].

A good deal of information can be retrieved in the example provided in Fig. 6a, where the complex permeability dependence on frequency is shown at three different J_p values in the representative case of the sample D1 tested at $T = 160$ °C. To start with, we highlight the decomposition of the complex permeability in its dw (μ'_{dw}, μ''_{dw}) and rotational (μ'_{rot}, μ''_{rot}) components. We make an estimate, based on the idea that $\mu''_{DC} = \mu''_{dw}$ at very low frequencies (W_{hyst} originating from dw motion only) and that any increase of the permeability under increasing J_p is due to the dw motion. This result is achieved by means of a simple procedure, described in detail in [17,20]. To note in Fig. 4a an early relaxation stage of μ(2mT) due to the aftereffect, which occurs in the very low (J_p –f) corner, followed by the main relaxation of μ_{dw} around some hundred kHz. The dominant role of μ_{rot} versus μ_{dw} up to 50 mT at $T = 160$ °C is apparent. It is one main reason for the decrease of the loss with T at low frequencies.

One may wonder how rotations and dw motion coexist and interact in these low anisotropy materials. The inset in Fig. 6a draws a possible scenario, where a single grain immersed in a polycrystalline environment is occupied by an array of 180° dws. The easy axis is misaligned with respect to the direction of the applied field $\boldsymbol{H}_a$ and the magnetization process proceeds under the effective field $\boldsymbol{H}_i$, the sum of the applied field and the demagnetizing field $\boldsymbol{H}_d$ arising at the grain boundary (disregarding the pinning field, $\boldsymbol{H}_i = \boldsymbol{H}_a + \boldsymbol{H}_d$). In the equilibrium configuration $\boldsymbol{H}_i$ is normal to the 180° dws and, at least for small fields, the rotation angle φ is the same in the opposite domains and the walls are not charged. Domain wall displacements cannot evidently proceed independent of spin rotations in the bulk, but by suffering

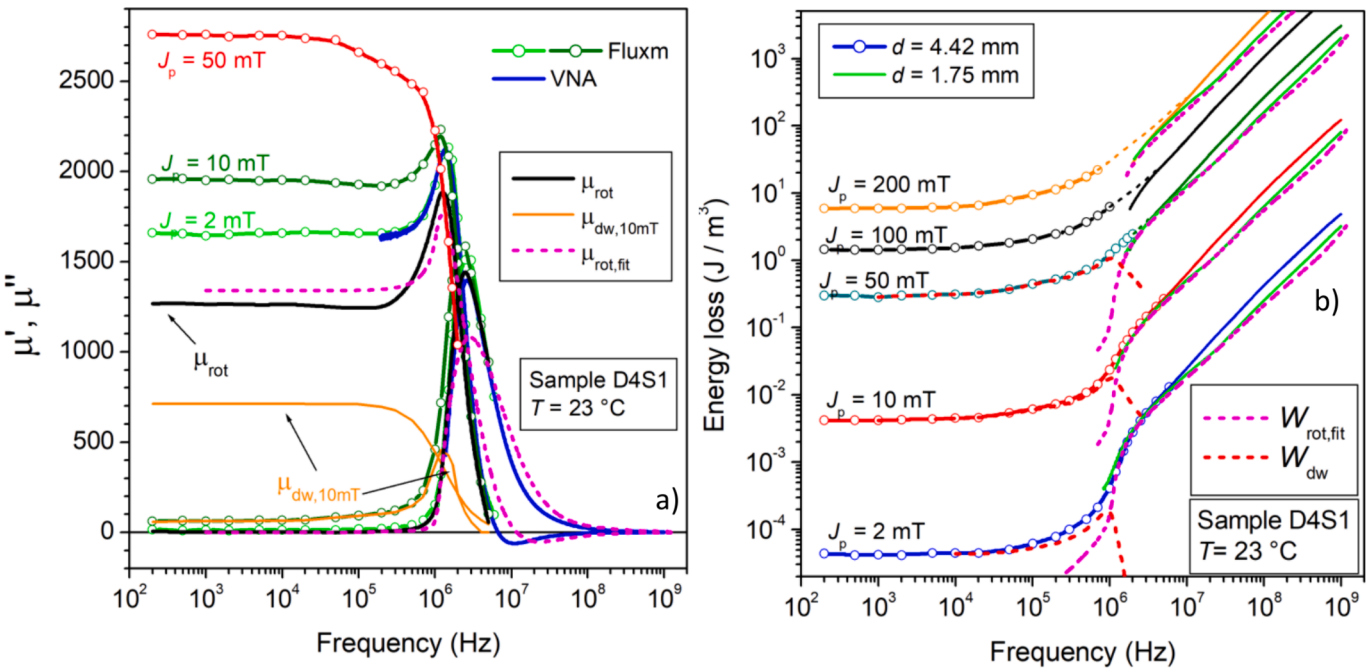

Fig. 7. Permeability decomposition (a) and energy loss up 1 GHz (b) in the Mn-Zn ferrite sample D4S1 at room temperature. The real and imaginary rotational permeabilities $\mu'_{rot}(f)$ and $\mu''_{rot}(f)$ are singled out of the measured permeabilities following the procedure discussed in [17,20]. The dw components $\mu'_{dw}(f)$ and $\mu''_{dw}(f)$ are responsible for the increase of the DC permeability with J_p, but they will eventually relax and vanish at the highest frequencies. $\mu'_{rot}(f)$ and $\mu''_{rot}(f)$ are theoretically predicted (dashed lines) as solutions of the Landau-Lifshitz equation with distributed anisotropy fields (i.e. resonant frequencies). The rotational loss $W_{rot,sd}$ is correspondingly predicted, for any J_p value, by use of Eq. (6) and the dw contribution $W_{dw}(f)$ is obtained as $W(f) - W_{rot,sd}(f)$ (dashed lines in (b)).

higher frictional effects under increasing frequencies, they will progressively give way, even at relatively high inductions, to spin rotations.

3.3. Anisotropy and effect of doping

The results and the analysis of the permeability behavior versus J_p and f are mirrored in the parallel phenomenology of the energy losses, shown up to 1 GHz, for J_p ranging between 2 mT and 200 mT, in Fig. 6b. The bifurcation of the $W(f)$ curves from ~ 5 MHz upward, signals the difference between the eddy current loss contributions in 5.02 mm and 1.77 mm thick samples. We also observe the additional loss generated by the magnetic aftereffect at the lowest frequencies ($J_p = 2$ mT), as well as the merging of the fluxmetric and VNA $W(f)$ curves (the latter being obtained under defined 10 mW incident power) occurring along an overlapping frequency range, inevitably shrinking with increasing J_p. This proves that, whatever J_p, the dws will sooner or later be fully damped in favor of rotations in their high-frequency motion. This is what the theoretical $\mu'_{rot}(f)$, $\mu''_{rot}(f)$, and $W_{rot,sd}(f)$ calculations predict (dashed lines in Fig. 6a and 6b). Modeling of the rotational processes, fully discussed with examples in [17,20], starts from the derivation of $\mu'_{rot}(f)$, and $\mu''_{rot}(f)$ as solutions of the Landau-Lifshitz equation for a suitable distribution (via a lognormal function) of the effective anisotropy fields, combination of magnetocrystalline and internal demagnetizing fields, around $< K_{eff} >$. The correspondingly identified spectrum of ferromagnetic resonance frequencies, associated with the dispersion of $\mu'_{rot}(f)$, $\mu''_{rot}(f)$ (Fig. 6a), culminates, for given J_p value, in the frequency-distributed energy loss.

$$W_{rot,sd}(J_p, f) = \pi J_p^2 \bullet \mu''_{rot}(f)/(\mu'^2(f) + \mu''^2(f)) \ [J/m^3] \quad (7)$$

It is remarked that we can provide physical meaning to the loss experiments only by keeping J_p constant versus frequency. Consequently, $\mu''(f)$ alone cannot be taken as representative of the measured loss, as it would be by keeping constant the peak applied field, according to the standard formulation $W(H_p, f) = \pi H_p^2 \bullet \mu''(f)$.

Examples of $W_{rot,sd}(f)$ predicted curves (dashed lines) are shown in Fig. 6b. Further examples (sample D4S1, $T = 23$ °C) are provided in Fig. 7. To note that modeling of $W_{rot,sd}(f)$ beyond about 1 MHz takes into account the concurrent widening of the distribution of $< K_{eff} >$, as engendered by the progressive increase of the internal demagnetizing

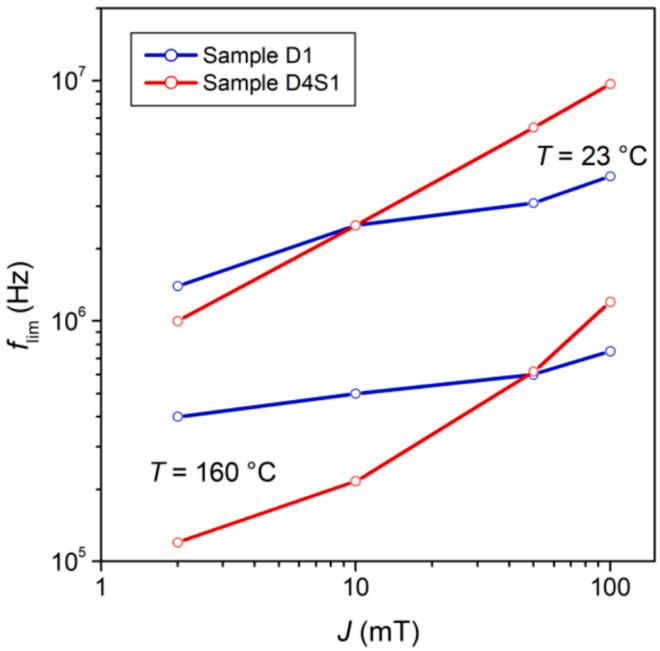

Fig. 8. The frequency f_{lim} at which the experimental $W(f)$ curves merge into the rotational loss curves $W_{rot,sd}(f)$ (see Figs. 6 and 7) increases with J_p, that is, with higher DC dw contribution. It therefore drops on passing from room temperature to 160 °C, because of the concurrent drop of $< K_{eff} >$. The $f_{lim}(J_p)$ line divides, at any temperature, the $(J_p - f)$ plane in a dw-prevalent (right portion) and in a rotation-prevalent (left portion) region.

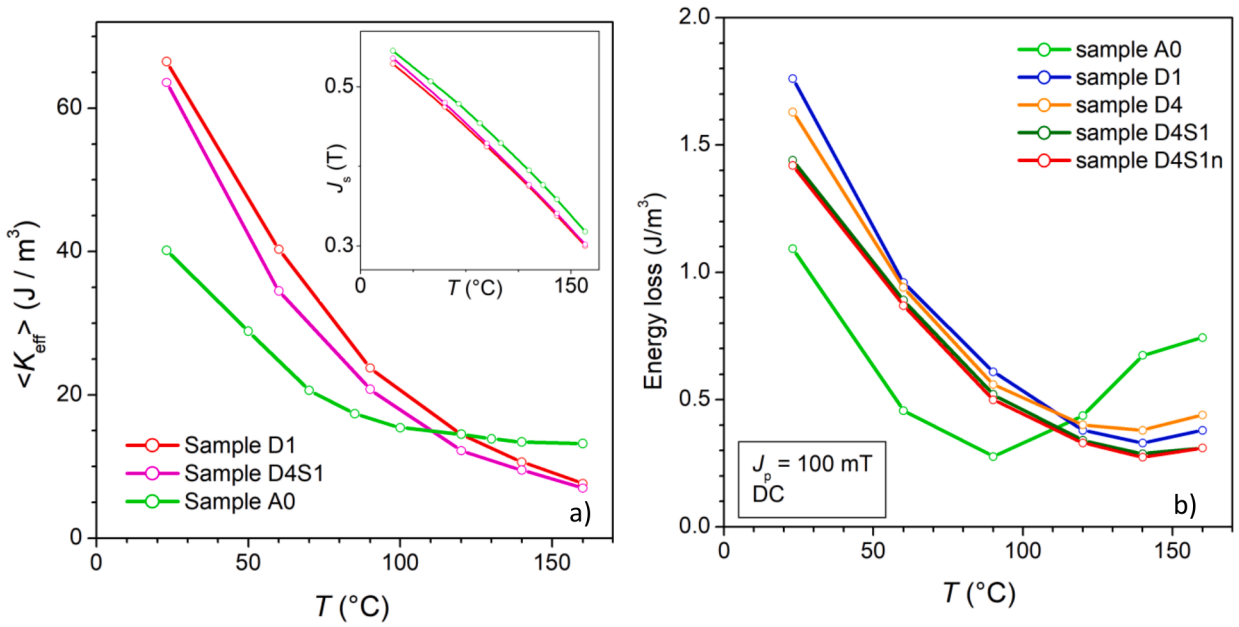

Fig. 9. a) The average effective anisotropy constant $< K_{eff} >$, obtained via Eq. (7) from the DC rotational permeability $\mu_{rot,DC}$, is observed to monotonically decrease with T up to 160 °C (samples D1 and D4S1). It is lower in the D4S1 sample ($SiO_2 = 50$ ppm) at all temperatures. The same quantity, obtained with the same procedure on a standard Mn-Zn ferrite (labelled A0), sintered at 1325 °C, shows instead restrained decrease of $< K_{eff} >$ at high temperatures. The attending dependence of J_s on T is provided in the inset. b) A parallel can be drawn between the $< K_{eff} >$ and the hysteresis (quasi-static) energy loss behaviours versus T, with the loss minimum delayed towards 150 °C in the novel materials and additional 50 ppm SiO_2 favouring better performance.

effects (see the related discussion in [17,20]). It is remarked that $\mu_{rot,DC}$ is largely prevalent at high temperatures, as justified by the decrease of $< K_{eff} >$ with T, according to expression for the initial rotational permeability with uniform angular distribution of easy axes

$$\mu_{rot,DC} = 1 + \frac{J_s^2}{3\mu_0 < K_{eff} >} \quad (8)$$

We can predict, at the same time, the dw permeability $\mu_{dw,DC} \propto J_s^2 / (\mu_0 < K_{eff} >^{1/2})$ [30]. A faster increase of $\mu_{rot,DC}$ versus $\mu_{dw,DC}$ is therefore envisaged for increasing T, notwithstanding the simultaneous decrease of J_s. Given the larger dynamic frictional effect suffered by the walls, the experimental $W(f)$ curves naturally end in the $W_{rot,sd}(f)$ curves at sufficiently high frequencies, as put in evidence by the examples illustrated in Figs. 6 and 7. The frequency f_{lim} at which merging occurs increases with J_p and decreases with T, because of the accompanying decrease of $< K_{eff} >$ (Fig. 8). We might conclude that, should one be able to push the anisotropy to vanishingly low values to favor the rotational processes, a loss advantage should always be reaped. This is true only to a point, however, because in doing so, we also move downward and widen the resonance frequency spectrum and the related energy absorption.

We observe that, in contrast with usually available Mn-Zn ferrites, the present materials exhibit monotonically decreasing losses till

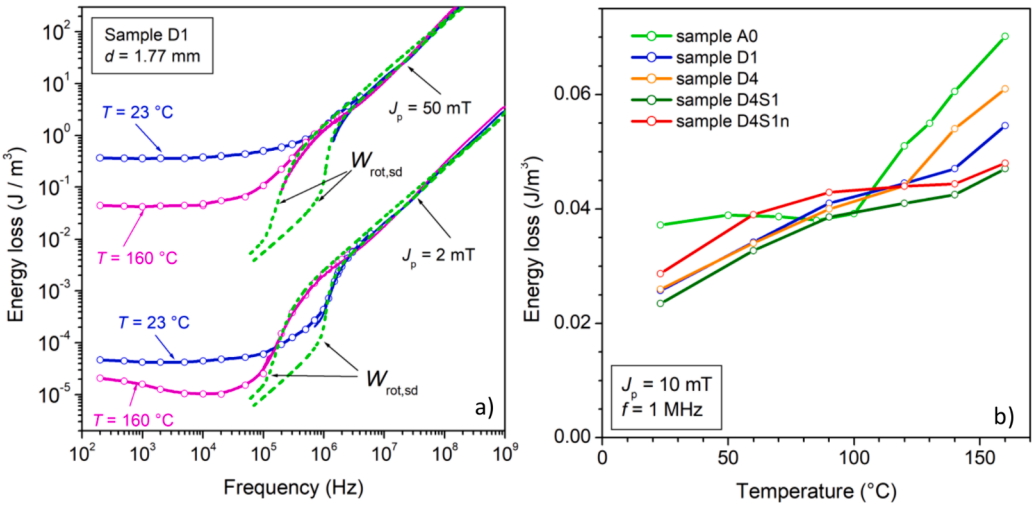

Fig. 10. The energy loss $W(f)$ measured up to 1 GHz in the thinned sample D1 at $T = 23$ °C and 160 °C is shown for $J_p = 2$ mT and 50 mT in association with the predicted rotational loss component $W_{rot,sd}(f)$ (broken lines). The dw contribution $W_{dw}(f)$ is not shown here for simplicity. The theoretical curves are calculated by taking into account that the distribution of the local (i.e. grain limited) effective anisotropies (an assumed lognormal function) broadens towards lower $< K_{eff} >$ values with increasing temperature (Fig. 9). They show that $W_{rot,sd}(f)$ can remarkably increase with T, between 100 kHz and 1 MHz, thereby justifying the measured increase of $W(f)$, when the (J_p, f) coordinate is above the $f_{lim}(J_p)$ curve of Fig. 8 (low J_p values). This is what is shown to occur in (b), where the increasing trend of $W(f)$ with T takes place, under the previous conditions, as a general property of the Mn-Zn ferrites.

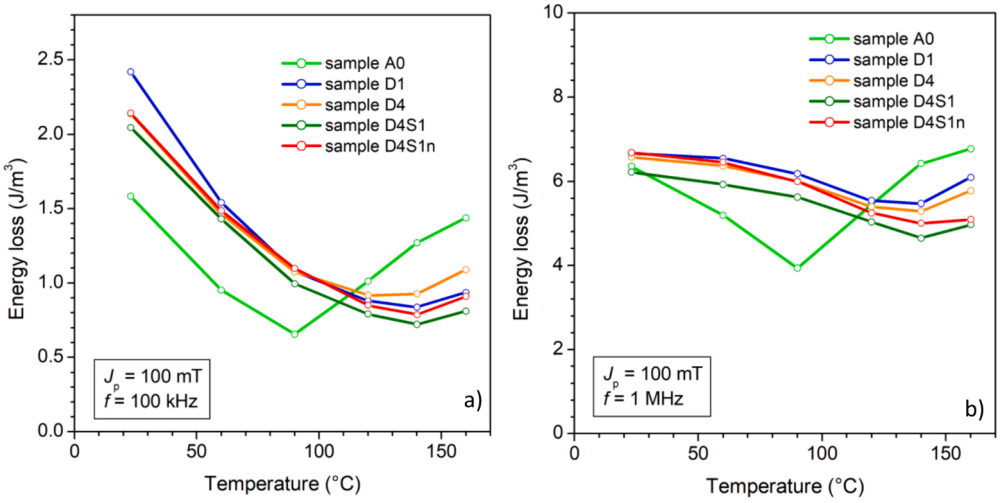

Fig. 11. a) The energy loss measured at $J_p = 100$ mT and $f = 100$ kHz is almost exclusively generated by the dw motion, as induced by the behaviour of the $W(f)$ curves and the theoretical $W_{rot,sd}(f)$ curves (Figs. 6 and 7). It is therefore bound to decrease with T, following the decrease of $< K_{eff} >$. b) The transition towards the rotational regime and the $W_{rot,sd}(f)$ increasing with T bring about levelling of the $W(T)$ curves at 1 MHz.

temperatures around 150 °C, a property that one can connect with a similar decrease of $< K_{eff} >$. Exploiting our capability to single $\mu_{rot,DC}$ out of the measured permeability, we arrive in fact at the dependence of $< K_{eff} >$ on temperature using Eq. (8). Fig. 9 shows then that the temperature dependence of the so-calculated $< K_{eff} >$, monotonically decreasing till 160 °C, is paralleled by the behavior of $W_{hyst}(T)$ for $J_p =$ 100 mT. The comparison made with the same quantities measured in a standard CaO and Nb_2O_5 doped Mn-Zn ferrite (labelled A0), sintered at 1325 °C (see [31]), makes clear how the minimum of W_{hyst}, displaced towards 150 °C on passing from sample A0 to the present Mn-Zn ferrites, correlates with the anisotropy behavior shown in Fig. 9a. The connection is noted between the D1 and D4S1 properties, where $< K_{eff} >$ and $W_{hyst}(T)$ are both lower in D4S1 and similar in their trend versus T. The general phenomenology cannot, however, be confined to the previous direct relationship of $W_{hyst}(T)$ with $< K_{eff} >$, although a loss advantage of the materials listed in Tables 1 and 2 with respect to the standard Mn-Zn ferrites is always observed under all ($J_p - f$) conditions for $T >$ 100–110 °C. The decisive factor in the $W(f)$ behavior versus J_p and T is the proportion existing between the dw and the rotational contributions to the dissipative process at any frequency, the dividing line between their respective hegemony in the ($J_p - f$) plane being given by $f_{lim}(J_p)$. One can observe in Fig. 8 how the passage from room temperature to 160 °C moves $f_{lim}(J_p)$ downward by about an order of magnitude, widening the ($J_p - f$) domain (upper region) where $W_{rot,sd}(f)$ mostly contributes to the loss.

With prevalent W_{dw} contribution, $W(f)$ is bound to decrease with T, at least before attaining the compensation temperature (generally far from the Curie point), as demonstrated by the W_{hyst} vs. T curves in Fig. 9b. The rotational loss, deriving from the dissipation of energy engendered by the ferromagnetic resonance, critically depends on the distribution of the resonance frequency $f_0 = (1/2\pi)\cdot\gamma\mu_0 H_{k,eff}$, that is, of the effective anisotropy field $H_{k,eff} = 2\,K_{eff}/J_s$, which broadens towards lower values at higher temperatures. We therefore predict the increase of $W(f)$ occurring, for example, between 100 kHz and 2.5 MHz in D1 for $J_p = 2$ mT following the increase of T from 23 °C to 160 °C (Fig. 10a), as due to additional contribution to $W_{rot,sd}(f)$ arising from broadened resonance energy absorption. It is observed in Fig. 10b that the increase of $W(f)$ with T is a general feature of all the investigated ferrite samples for $J_p = 10$ mT and $f = 1$ MHz. It is concluded that, where $W_{rot,sd}(f)$ dominates, $W(f)$ can only increase with T. In other words, any increase of temperature moves downward the $f_{lim}(J_p)$ curve in Fig. 8, thereby restricting the ($J_p - f$) domain where $W_{dw}(f)$ prevails upon $W_{rot,sd}(f)$ and $W(f)$ is bound to decrease with T. Fig. 11 shows instead how the

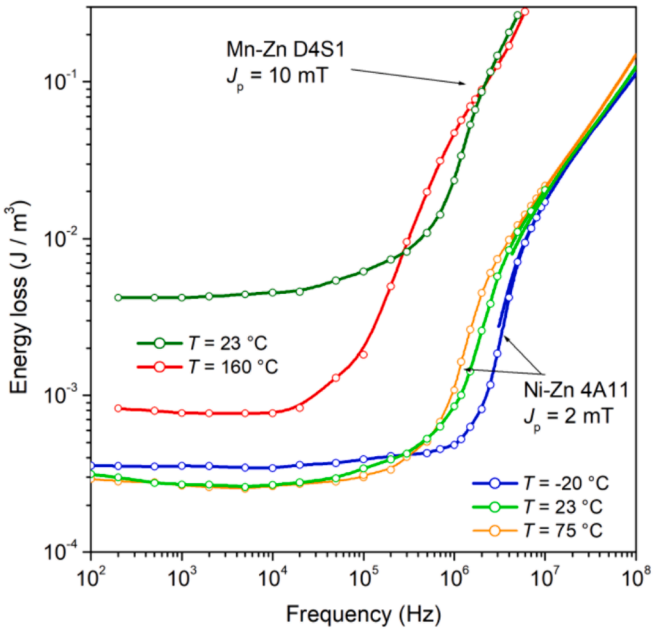

Fig. 12. The energy loss measured at $J_p = 2$ mT in the high-resistivity Ni-Zn sintered ferrite 4A11 ($\rho \sim 10^5$ Ωm) exhibits a similar temperature response as the Mn-Zn ferrites when the loss mechanism chiefly involves the rotational processes.

prevailing contribution by dw displacements occurring at 100 kHz for J_p = 100 mT engenders a rapid decrease with T of $W(f)$ following the similar decrease of $< K_{eff} >$. On attaining $f = 1$ MHz, the dw relax their contribution in favor of rotations and the $W(f)$ vs. T curves are smoothed out.

It might be argued that the previously discussed sharp increase of $W(f)$ with T at intermediate frequencies and low J_p values could possibly arise from eddy currents, ensuing from the accompanying rapid surge of the material conductivity (see Fig. 5b). Such a possibility is excluded by the model and the experiments. It is a specific property of rotations and the related resonant dissipation by spin damping in ferrites, an effect shared in fact by the highly insulating ($\rho \sim 10^5$ Ωm) Ni-Zn sintered ring samples, as demonstrated by the compared $W(f)$ behaviors in Fig. 12.

A certain trend in the response of the differently doped samples is

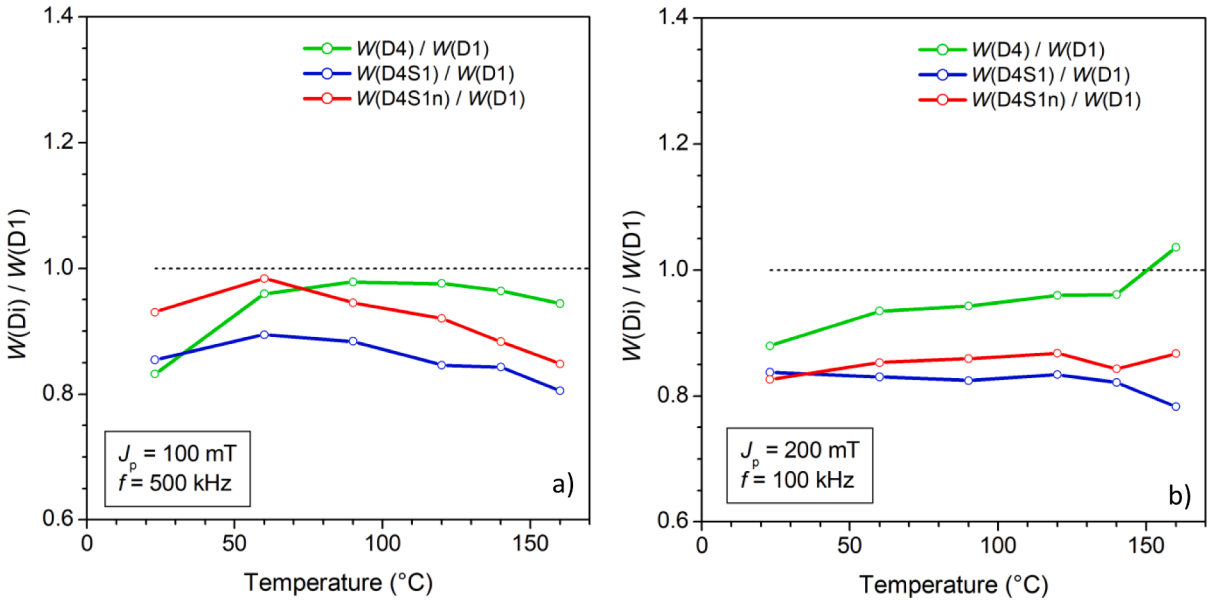

Fig. 13. For suitably high values of the peak polarization J_p, the dw contribution $W_{dw}(f)$ to the measured loss overcomes the rotational contribution $W_{rot,sd}(f)$ at low and medium frequencies and $W(f)$ decreases with decreasing anisotropy $< K_{eff} >$ (Fig. 9). Under these circumstances, extra-doping made in samples D4 and D4S1 (Table 1) appears to favourably affect the material properties, in comparison with the starting standard ferrite D1, with about 20 % decrease of $W(f)$.

observed in Figs. 9-11, which is substantiated by the systematic investigation performed over a large matrix of ($J_p - f$) coordinates. We have verified in Fig. 9a, via the analysis of μ_{rot}, that extra-doping up to 50 ppm Si leads to a certain decrease of $< K_{eff} >$ at all temperatures (comparison between D1 and D4S1). We consequently expect a favorable effect on $W(f)$, whenever W_{dw}(f) plays a major role, that is, at sufficiently high J_p values and medium frequencies. Fig. 13 demonstrate that under these circumstances the proposed extra-doped samples D4, D4S1, and D4S1n (Table 1) exhibit generally lower energy loss with respect to the standard material D1.

4. Conclusions

This work has been devoted to the measurement and the physical assessment of the broadband complex permeability and energy losses of Mn-Zn ferrite samples prospectively suited for applications at high temperatures. A comprehensive magnetic characterization has been performed, from DC to 1 GHz, up to 160 °C, with accompanying measurements of the complex electrical resistivity. Increased doping by CaO, Nb_2O_5, ZrO_2, and SiO_2 is shown to favor to some degree loss reduction at all temperatures. This appears to depend, for any ($J_p - f$) coordinate, on the degree by which the domain wall displacements and the rotation-precession of the magnetic moments in the bulk share the magnetization reversal. The resulting temperature-dependent phenomenology has been assessed in this work by relying on the general concept of loss decomposition, generalized to semi-insulating materials, and can be summarized according to the following lines: 1) The eddy currents provide a recognizable contribution to the losses only at very high frequencies, beyond a few MHz. This frequency limit is expected to move towards lower frequencies only for increasing sample size and thickness well above the present case [14]. 2) Rotational and dw permeabilities are experimentally separated and the associated loss figures $W_{rot,sd}(f)$ and $W_{dw}(f)$ are identified. With the rotational loss calculated via the Landau-Lifshitz equation and the related complex permeability predicted under assumed distribution of local magnetic anisotropies, it is verified that $W_{dw}(f)$ and $W_{rot,sd}(f)$ predominantly cover the lower and upper frequency ranges, respectively. 3) The effective magnetic anisotropy $< K_{eff} >$ is calculated and shown to monotonically decrease with T, with contrasting effects on $W_{dw}(f)$ and $W_{rot,sd}(f)$. The rotational losses always increase with T, because the local resonance frequencies (and the associated dissipative process), proportionally related to K_{eff}, broaden their distribution towards lower f values. The opposite occurs for $W_{dw}(f)$. The loss can therefore decrease with T only for those ($J_p - f$) values where $W_{dw}(f)$ predominates. 4) A dividing f_{lim} (J_p) line between dominant $W_{dw}(f)$ or $W_{rot,sd}(f)$ domains is identified in the ($J_p - f$) plane. It moves downward with increasing T, shrinking the favorable $W_{dw}(f)$ governed region; 5) Increased doping appears to indirectly affect $< K_{eff} >$ and lead, in the appropriate ($J_p - f$) domain, to a moderate (20 – 30 %) decrease of $W(f)$ at all temperatures.

CRediT authorship contribution statement

Vasiliki Tsakaloudi: Writing – review & editing, Investigation, Conceptualization. **Cinzia Beatrice:** Writing – review & editing, Methodology, Investigation, Data curation. **Fausto Fiorillo:** Writing – original draft, Methodology, Formal analysis, Conceptualization. **Vassilios Zaspalis:** Writing – review & editing, Conceptualization.

Declaration of competing interest

The authors declare that they have no known competing financial interests or personal relationships that could have appeared to influence the work reported in this paper.

Data availability

Data will be made available on request.

Acknowledgments

This work was performed in the context of the Agreement of Scientific and Technological Cooperation between the Istituto Nazionale di Ricerca Metrologica (INRIM) and The Centre for Research and Technology Hellas (CERTH) regarding the study of soft ferrites.

The authors acknowledge the precious help of Dr. Enzo Ferrara, at INRIM, in the measurements.

Appendix A. Supplementary data

Supplementary data to this article can be found online at https://doi.org/10.1016/j.jmmm.2024.172228.

References

[1] V.T. Zaspalis, E. Eleftheriou, The effect of TiO2 on the magnetic power losses and electrical resistivity of polycrystalline MnZn ferrites, J. Phys. d: Appl. Phys. 38 (2005) 2156–2161, https://doi.org/10.1088/0022-3727/38/13/0123.

[2] H. Shokrollahi, K. Janghorban, Influence of additives on the magnetic properties, microstructure and densification of Mn-Zn soft ferrites, Mater. Sci. Eng. B 141 (2007) 91–107, https://doi.org/10.1016/j.mseb.2007.06.005.

[3] S.F. Wang, Y.J. Chiang, Y.F. Hsu, C.H. Hsen, Effects of additives on the loss characteristics of Mn-Zn ferrites, J. Magn. Magn. Mater. 365 (2014) 119–125, https://doi.org/10.1016/j.jmmm.2014.04.043.

[4] S. Tokatlidis, K. Kogias, V.T. Zaspalis, Low loss Mn-Zn ferrites for applications in the frequency region of 1–3 MHz, J. Magn. Magn. Mater. 465 (2018) 727–735, https://doi.org/10.1016/j.jmmm.2018.06.056.

[5] A. Žnidaršič, M. Drofenik, High-resistivity grain boundaries in CaO-doped MnZn ferrites fot high-frequency power applications, J. Am. Ceram. Soc. 82 (1999) 359–365, https://doi.org/10.1111/j.1551-2916.1999.tb20070.x.

[6] K. Jiang, K. Li, C. Peng, Y. Zhu, Effect of multi-additives on the microstructure and magnetic properties of high-permeability Mn–Zn ferrite, J. Alloys Comp. 541 (2012) 472–476, https://doi.org/10.1016/j.jallcom.2012.06.113.

[7] V. Loyau, G.-Y. Wang, M. Lo Bue, F. Mazaleyrat, An analysis of Mn-Zn ferrite microstructure by impedance spectroscopy, scanning transmission electron microscopy and energy dispersion spectrometry characterizations, J. Appl. Phys. 111 (2012) 053928, https://doi.org/10.1063/1.3693544.

[8] B. Sun, F. Chen, W. Yang, H. Shen, D. Xie, Effects of nano-TiO_2 and normal size TiO_2 on the microstructure and magnetic properties of manganese-zinc power ferrites, J. Magn. Magn. Mater. 349 (2014) 180–187, https://doi.org/10.1016/j.jmmm.2013.09.006.

[9] L. Li, Z. Lan, Z. Yu, K. Sun, Z. Xu, Effects of Co-substitution on wide temperature ranging characteristic of electromagnetic properties in MnZn ferrites, J. Alloys Comp. 476 (2009) 755–759, https://doi.org/10.1016/j.jallcom.2008.09.101.

[10] A. Fujita, S. Gotoh, Temperature dependence of core loss in Co-substituted MnZn ferrites, J. Appl. Phys. 93 (2003) 7477–7479, https://doi.org/10.1063/1.1557952.

[11] C. Beatrice, S. Dobák, V. Tsakaloudi, C. Ragusa, F. Fiorillo, The temperature dependence of magnetic losses in CoO-doped Mn-Zn ferrites, J. Appl. Phys. 126 (2019) 143902, https://doi.org/10.1063/1.5118824.

[12] H.N. Ji, Z.W. Lan, Z. Yu, et al., Microstructure and temperature dependence of magnetic properties of MnZnTiSn ferrites for power applications, IEEE Trans. Magn. 46 (2010) 974–978, https://doi.org/10.1109/TMAG.2009.2037954.

[13] M. Gu, G.Q. Liu, Effects of MoO_3 and TiO_2 additions on the magnetic properties of manganese–zinc power ferrites, Journal of Alloys and Compounds 475 (2009) 356–360, https://doi.org/10.1016/j.jallcom.2008.07.043.

[14] F. Fiorillo, C. Beatrice, O. Bottauscio, E. Carmi, Eddy current losses in Mn-Zn ferrites, IEEE Trans. Magn. 50 (2014) 6300109, https://doi.org/10.1109/TMAG.2013.2279878.

[15] T. Dimier, J. Biela, Eddy current loss model for ferrite ring cores based on a metamaterial model of the core properties, IEEE Trans. Magn. 58 (2022) 6300605, https://doi.org/10.1109/TMAG.2021.3084812.

[16] G. Bertotti, *Hysteresis in Magnetism*, Academic Press: San Diego, CA, USA, 1998; pp. 391–430.

[17] S. Dobák, C. Beatrice, V. Tsakaloudi, F. Fiorillo, Magnetic Losses in Soft Ferrites, Magnetochemistry 8 (2022) 60, https://doi.org/10.3390/magnetochemistry8060060.

[18] J. Reinert, A. Brockmeyer, R.W. De Doncker, Calculation of losses in ferro- and ferrimagnetic materials based on the modified Steinmetz equation, IEEE Trans. Ind. Appl. 37 (2001) 1055–1061, https://doi.org/10.1109/28.936396.

[19] J. Mülethaler, J. Biela, J.W. Kolar, A. Ecklebe, Core losses under the DC bias condition based on Steinmetz parameters, IEEE Trans. Power. Electron. 27 (2012) 953–963, https://doi.org/10.1109/TPEL.2011.2160971.

[20] C. Beatrice, V. Tsakaloudi, S. Dobák, V. Zaspalis, F. Fiorillo, Magnetic losses versus sintering treatment in Mn-Zn Ferrites, J. Magn. Magn. Mater. 429 (2017) 129–137, https://doi.org/10.1016/j.jmmm.2016.12.121.

[21] F. Fiorillo, Measurements of magnetic materials, Metrologia 47 (2010) S114–S142, https://doi.org/10.1088/0026-1394/47/2/S11.

[22] J. Smit, H.P.J. Wijn, Ferrites, Philips Technical Library, Eindhoven, 1959, p. 229.

[23] D. Ravinder, K. Latha, Electrical conductivity of Mn-Zn ferrites, J. Appl. Phys. 75 (1994) 6118–6120, https://doi.org/10.1063/1.355479.

[24] C. Fiorillo, O. Beatrice, M.C. Bottauscio, A. Manzin, An approach to magnetic losses and their frequency dependence in Mn-Zn ferrites, Appl. Phys. Lett. 89 (2006) 122513, https://doi.org/10.1063/1.2356111.

[25] J.C. Peuzin, Les matériaux doux pour l'électronique haute fréquence, in *Magnétisme*, vol. II, E. du Trémolet de Lachisserie, ed., Presses Universitaires de Grenoble (1999), p. 155.

[26] O. de la Barrière, C. Appino, F. Fiorillo, C. Ragusa, M. Lecrivain, L. Rocchino, H. Ben Ahmed, M. Gabsi, F. Mazaleyrat, M. LoBue, Characterization and prediction of magnetic losses in Soft Magnetic Composites under distorted induction waveforms, IEEE Trans. Magn. 49 (2013) 1318–1326, https://doi.org/10.1109/TMAG.2012.2218614.

[27] W.H. Jeong, B.M. Sung, Y.H. Han, Analysis of power losses in Mn-Zn ferrites, Jap. J. Appl. Phys. 41 (2002) 2912–2915, https://doi.org/10.1143/JJAP.41.2912.

[28] J. Töpfer, A. Angermann, Complex additive systems for Mn-Zn ferrites with low power loss, J. Appl. Phys. 117 (2015) 17A504, https://doi.org/10.1063/1.4918692.

[29] J.B. Goodenough, Summary of losses in magnetic materials, IEEE Trans. Magn. 38 (2002) 3398–3408, https://doi.org/10.1109/TMAG.2002.802741.

[30] F. Fiorillo, C. Appino, and M. Pasquale, Hysteresis in magnetic materials, in *The Science of Hysteresis*, vol. III, G. Bertotti and I. Mayergoyz, eds., Elsevier (2006), p. 62.

[31] C. Beatrice, S. Dobák, V. Tsakaloudi, C. Ragusa, F. Fiorillo, L. Martino, and V. Zaspalis, AIP Advances 8 (2018) Article n° 047803. 10.1063/1.4993718.